NOVEMBER 1987   PETER R. GENT   1897

Forcing and Friction Effects on Vertically Propagating Waves in the Equatorial Oceans

PETER R. GENT

National Center for Atmospheric Research, Boulder, CO 80307

(Manuscript received 20 November 1986, in final form 20 March 1987)

ABSTRACT

In this paper the linear equatorial ocean response to stress forcing is analyzed in terms of vertically propagating waves. A new projection onto the meridional eigenfunctions of the pressure equation is derived for a single Fourier wave component. The projection demonstrates that the solution is regular and not singular at the inertial latitudes, and is more convenient to use than the corresponding projection onto the meridional velocity equation. The wavenumber spectrum from the resulting forced vertical structure equation is found for four different choices of the vertical profile for the body force. The spectrum is shown to be insensitive to the particular profile chosen. The projection is then used to study the effects of forcing and linear damping on the vertical propagation of space–time transformed energy in three wave modes: the Kelvin, first Rossby and mixed Rossby–gravity waves. When the buoyancy frequency is constant, the energy decay is exponential in depth with the coefficient proportional to the damping magnitude. Finally it is shown that linear damping effects are very different on each vertically propagating or vertically standing wave. Thus, it is fallacious to make deductions about meridional phase changes in the total solution to a general forced problem from the phase changes of each wave component.

1. Introduction

The problem of how energy propagates vertically and horizontally is crucial to understanding the response of both the upper and deep equatorial ocean to stress and thermal forcing. Forcings have broad spectra in time and space, the dissipation in the upper equatorial oceans (as well as the mixed layer response) is only now beginning to be measured, and all of these factors are important to understanding how well energy propagates vertically. In observations there is evidence of vertical energy propagation (see section 2 of Gent and Luyten, 1985, for a summary) and of strong horizontal propagation. A Kelvin wave traversing the Pacific is documented in Knox and Halpern (1982), and Lukas et al. (1984) analyze the sea level response in the Pacific in 1982–83 and show very strong horizontal coherence. Model studies have also given evidence of both vertical and horizontal energy propagation. Rothstein et al. (1985) conclude that strong vertical propagation occurs for a periodically forced Kelvin wave, whereas Gent and Luyten (1985) conclude that strong reflection of energy off the thermocline can occur. In the latter paper (p. 1006) is a discussion of three other factors that affect the vertical propagation of energy: (i) the time and horizontal spatial structure of the wind stress forcing of the ocean; (ii) how the wind stress drives the ocean or the vertical profile assumed for the body force; and (iii) the strength of friction. This paper attempts to address the effects of these three factors using the simplifying assumptions of no mean flow and a constant buoyancy frequency so that the effects can be found analytically.

Two approaches can be used to construct forced linear equatorial solutions: the vertically standing (VS) representation and the vertically propagating (VP) representation. The most comprehensive discussion of the two representations for forced oceanic waves is by Philander (1978). Nearly all forced linear equatorial ocean solutions to date have been calculated using the VS representation. Here the forcing is first projected onto the vertical eigenfunctions of the ocean, and then for each vertical mode the horizontal solution is calculated. Finally the vertical mode solutions are summed to obtain the total solution. Using the VS representation, the vertical propagation of energy is not clear until the total solution is obtained because there is no vertical propagation in each of the wave components. In contrast, most forced linear tropical atmosphere solutions are calculated using the VP representation. Now the forcing is first projected onto the meridional eigenfunctions of the globe, and then for each meridional mode the vertical solution is calculated. Finally the meridional mode solutions are summed to obtain the total solution. In the VP representation, the vertical propagation of energy is more transparent because it is calculated explicitly for each space–time Fourier transformed wave. The VP representation used in this paper was stimulated by Salby and Garcia (1987) who use a similar method to calculate the global atmospheric response to tropical heat forcing.

The plan of the paper is as follows. In section 2 a new projection onto the meridional eigenfunctions of the pressure equation is derived allowing stress forcing to be incorporated into the VP representation. Then the wavenumber spectrum from the forced vertical

© 1987 American Meteorological Society

equation is found for four different profiles for the body force. The response to particular stress forcings is calculated in section 3. The effects of forcing and friction on the vertical propagation of space–time transformed energy of the Kelvin, first Rossby and mixed Rossby–gravity waves are then studied. Section 4 shows that linear damping effects on each VP or VS wave are very different. Section 5 contains the discussion and conclusions.

2. Vertically propagating wave formulation

The hydrostatic, Boussinesq, inviscid primitive equations linearized about a state of no motion are

$$u_t - fv + p_x = \tau_z{}^x \qquad (1)$$

$$v_t + fu + p_y = \tau_z{}^y, \qquad (2)$$

$$p_z + g\rho = 0, \qquad (3)$$

$$\rho_t - N^2 w/g = 0, \qquad (4)$$

$$u_x + v_y + w_z = 0 \qquad (5)$$

where u, v and w are velocities; p, ρ and τ are pressure, density and the wind stress all divided by a reference density; g is gravity; and N the buoyancy frequency. On an equatorial β-plane, the Coriolis frequency f takes the form

$$f = \beta y. \qquad (6)$$

If (1) to (5) are Fourier transformed in time and longitude, then a single Fourier component with frequency σ and zonal wavenumber k is considered. Eliminating v and u between (1) and (2) and ρ between (3) and (4) gives equations for the velocities in terms of pressure:

$$(\sigma^2 - f^2)u = fp_y + \sigma kp + i\sigma\tau_z{}^x - f\tau_z{}^y, \qquad (7)$$

$$(\sigma^2 - f^2)v = -i\sigma p_y - ikfp + f\tau_z{}^x + i\sigma\tau_z{}^y, \qquad (8)$$

$$w = i\sigma p_z/N^2. \qquad (9)$$

These expressions can be substituted into the continuity equation (5) to give the following equation for pressure:

$$\left[\frac{p_y}{(\sigma^2 - f^2)}\right]_y + \left\{\left[\frac{kf}{\sigma(\sigma^2 - f^2)}\right]_y - \frac{k^2}{(\sigma^2 - f^2)}\right\}p - \left[\frac{p_z}{N^2}\right]_z$$

$$= \frac{i}{\sigma}\left\{\frac{k}{(\sigma^2 - f^2)}(\sigma\tau_z{}^x + if\tau_z{}^y) - \left[\frac{f\tau_z{}^x + i\sigma\tau_z{}^y}{(\sigma^2 - f^2)}\right]_y\right\}. \qquad (10)$$

This equation is separable into horizontal and vertical components providing the stress and boundary conditions are also separable. In the VP representation, the solution is now projected onto the eigenfunctions of the horizontal operator of (10) which satisfy the equation

$$\left[\frac{p_y}{(\sigma^2 - f^2)}\right]_y + \left\{\left[\frac{kf}{\sigma(\sigma^2 - f^2)}\right]_y - \frac{k^2}{(\sigma^2 - f^2)}\right\}p + \frac{p}{gh} = 0,$$

$$(11)$$

where gh is the eigenvalue. If an equation is formed in v instead of p, then the corresponding horizontal eigenfunctions satisfy the parabolic cylinder equation:

$$v_{yy} - \left(k^2 + \frac{\beta k}{\sigma}\right)v + (\sigma^2 - f^2)\frac{v}{gh} = 0. \qquad (12)$$

The eigenfunctions of (11) and (12) can be separated into two sets. When gh is positive they are the familiar Hermite function solutions:

$$P^n = \sqrt{gh^n}[\sqrt{2(n+1)}a_n\psi_{n+1}(y') - \sqrt{2n}b_n\psi_{n-1}(y')],$$

$$V^n = \frac{2\sigma}{i}\left(\frac{gh^n}{\beta^2}\right)^{1/4}\psi_n(y'),$$

$$U^n = [\sqrt{2(n+1)}a_n\psi_{n+1}(y') + \sqrt{2n}b_n\psi_{n-1}(y')], \qquad (13)$$

where ψ_n is the Hermite function of degree n

$$\psi_n(y') = H_n(y')e^{-y'^2/2}/(2^n n!)^{1/2}\pi^{1/4}, \quad y' = \left(\frac{\beta^2}{gh^n}\right)^{1/4}y,$$

$$a_n^{-1} = 1/\sqrt{gh^n} - k/\sigma, \quad b_n^{-1} = 1/\sqrt{gh^n} + k/\sigma. \qquad (14)$$

The eigenvalues are given by the dispersion relation

$$\left(k^2 + \frac{\beta k}{\sigma}\right)gh^n + \sqrt{gh^n}\beta(2n+1) - \sigma^2 = 0. \qquad (15)$$

There is also a less familiar set of eigenfunctions when gh is negative. These solutions of (11) and (12) are exponential equatorward of the inertial latitude and damped oscillatory poleward of it: exactly the opposite of the Hermite functions. They are bounded at infinity where they have $y^{-1/2}$ algebraic decay; see Abramowitz and Stegun (1964, p. 693).

a. Horizontal projection

The pressure is now expressed as a sum over all the eigenfunctions P^n

$$p = \sum_n p^n(z)P^n(y), \qquad (16)$$

and (10) is then projected onto the eigenfunction P^n. The P^n are orthogonal so that the projection gives the following equation for p^n:

$$\left\{\left[\frac{p_z{}^n}{N^2}\right]_z + \frac{p^n}{gh^n}\right\}\int_{-\infty}^{\infty}P^{n2}dy$$

$$= \frac{1}{i\sigma}\int_{-\infty}^{\infty}\left\{\frac{k}{(\sigma^2 - f^2)}(\sigma\tau_z{}^x + if\tau_z{}^y) - \left[\frac{f\tau_z{}^x + i\sigma\tau_z{}^y}{(\sigma^2 - f^2)}\right]_y\right\}P^n dy.$$

$$(17)$$

The projection of the forcing on the right-hand side of (17) appears to be singular at the inertial latitudes $y = \pm\sigma/\beta$ because of the $(\sigma^2 - f^2)$ terms in the denominator. This apparent singularity does not arise in the atmospheric situation when the forcing is in the heat equation; see Salby and Garcia (1987). It did arise in Wunsch (1977) who addressed the same problem as in

this section, but he did not mention the apparent singularity and avoided singular values by assumption rather than the derivation below. The eigenfunction equation for P^n, (11), also appears singular but its solution (13) is not. The inertial latitudes are, in fact, associated with removable singularities of (11); this is also true of the forcing projection and can be demonstrated by integrating the second term on the right-hand side of (17) by parts to obtain

$$\left\{\left[\frac{p_z^n}{N^2}\right]_z + \frac{p^n}{gh^n}\right\}\int_{-\infty}^{\infty} P^{n2}\,dy$$

$$= \frac{1}{i\sigma}\int_{-\infty}^{\infty}\left[\tau_z{}^x\frac{(\sigma k P^n + f P_y{}^n)}{(\sigma^2 - f^2)} + i\tau_z{}^y\frac{(k f P^n + \sigma P_y{}^n)}{(\sigma^2 - f^2)}\right]dy. \tag{18}$$

Comparing the resulting expressions with the unforced version of (7) and (8), which are the equations satisfied by U^n, V^n and P^n, shows that (18) can be written in the form:

$$\left[\frac{p_z^n}{N^2}\right]_z + \frac{p^n}{gh^n} = \frac{1}{i\sigma}\int_{-\infty}^{\infty}(\tau_z{}^x U^n - \tau_z{}^y V^n)dy \bigg/ \int_{-\infty}^{\infty} P^{n2}\,dy. \tag{19}$$

This projection equation is new and shows that the projection is regular at the inertial latitudes. The corresponding projection equation in terms of v is

$$\left\{\left[\frac{v_z^n}{N^2}\right]_z + \frac{v^n}{gh^n}\right\}\int_{-\infty}^{\infty}(\sigma^2 - f^2)V^{n2}\,dy$$

$$= \int_{-\infty}^{\infty}\left\{\left[\frac{f\tau_{zz}^x + i\sigma\tau_{zz}^y}{N^2}\right]_z + \frac{ik^2}{\sigma}\tau_z{}^y - \frac{k}{\sigma}\tau_{yz}^x\right\}V^n\,dy. \tag{20}$$

A comparison of (19) and (20) shows that the projection onto the p equation is simpler than onto the v equation and does not contain z derivatives of the forcing. The forcing projection onto the v equation contains two z derivatives, so it is difficult to apply if the body force is assumed discontinuous at the base of the forcing layer as is normally the case in the VS representation. It is also convenient to work with p because the velocities are more easily derived from it than from v [see (7)–(9)], and the p equation includes the Kelvin wave which the v equation does not.

b. Vertical solution

In order to solve the vertical structure equation (19) a vertical distribution for the body force has to be assumed. The usual assumption is that the body force acts uniformly over a depth d and not below. In this case (19) becomes

$$\left[\frac{p_z^n}{N^2}\right]_z + \frac{p^n}{gh^n} = A^n e(z), \tag{21}$$

where

$$e(z) = \begin{cases} 1, & d < z < 0 \\ 0, & z < d, \end{cases} \tag{22}$$

and A^n is a constant. For illustrative purposes and analytic tractability, the buoyancy frequency N is now assumed constant throughout the ocean. The solution to (21) is

$$p^n = gh^n A^n \begin{cases} 1 - e^{imd}\cos mz, & d < z < 0 \\ -ie^{imz}\sin md, & z < d, \end{cases}$$

$$m = \frac{N}{\sqrt{gh^n}}, \quad gh^n > 0, \tag{23}$$

or

$$p^n = gh^n A^n \begin{cases} 1 - (\sinh md + \cosh md)\cosh mz, \\ \qquad\qquad\qquad\qquad d < z < 0 \\ -\sinh md(\sinh md + \cosh md)e^{m(z-d)}, \\ \qquad\qquad\qquad\qquad z < d, \end{cases}$$

$$m = \frac{N}{\sqrt{-gh^n}}, \quad gh^n < 0. \tag{24}$$

This solution satisfies p_z^n (or w^n) zero at the surface, $z = 0$, p^n and p_z^n (or w^n) continuous at the base of the forcing layer, $z = d$, and either the radiation condition or decay in the deep ocean. The positive gh^n solution (23) is vertically propagating and has upward phase propagation in the deep ocean which implies downward energy propagation, whereas the negative gh^n solution (24) is trapped near the surface. These characteristics of the solution remain true if a) N is nonuniform, b) the forcing layer is assumed well mixed so that $N = 0$ down to depth d, and c) a free rather than a rigid upper surface is assumed.

The amplitude of the vertically propagating solution (23) in the deep ocean is

$$\frac{A^n N^2}{m^2}\sin md = \begin{cases} O(m^{-1}), & m \to 0 \\ O(m^{-2}), & m \to \infty. \end{cases} \tag{25}$$

Thus, solutions in the deep ocean will exhibit red spectra with respect to the vertical wavenumber m, because the solution amplitude will be dominated by the longest vertical wavelengths and be small for the shortest vertical wavelengths. A similar result is found in Salby and Garcia (1987), who show that the tropical stratospheric solution is red with respect to vertical wavenumber.[1]

One of the questions posed at the beginning of the paper is the sensitivity of the solution to various choices

---

[1] The $m \to 0$ solution is not singular as implied by (25) since A^n is a function of m. It is a different function for each wave component; see next section.

for the vertical distribution of the body force. In order to answer this question $e(z)$ is now given three different profiles:

$$1: \quad e^{bz}, \quad b \text{ large,}$$

$$2: \quad \begin{cases} \cos(\pi z/2d), & d<z<0 \\ 0, & z<d, \end{cases} \quad (26)$$

$$3: \quad \begin{cases} 1-z/d, & d<z<0 \\ 0, & z<d. \end{cases}$$

The amplitude of the vertically propagating solution below the forcing layer in these cases is

$$1: \quad A^n N^2 b/m(b^2+m^2),$$

$$2: \quad A^n N^2 \pi \, \cos md/2md\left(m^2 - \frac{\pi^2}{4d^2}\right), \quad (27)$$

$$3: \quad A^n N^2(\cos md - 1)/m^3 d.$$

All these amplitudes are such that

$$\text{Amplitudes} = \begin{cases} O(m^{-1}), & m \to 0 \\ O(m^{-3}), & m \to \infty, \end{cases} \quad (28)$$

except that the last two profiles tend to zero faster as $m \to \infty$ in the case when md is special multiples of π. Thus the behavior for all four profiles is the same in the important long wavelength limit, whereas the uniform body force in the forcing layer gives a slightly less red spectrum with slower decay than the other profiles in the short wavelength limit. This shows that the solution amplitudes in the deep ocean are insensitive to the precise choice of the body force distribution with depth because of the red character of the solution. This result is similar to one in Salby and Garcia (1987) who show in appendix B that the solution in the stratosphere is insensitive to the precise choice of heating profile with height in the troposphere.

3. Space–time transformed wave solutions

In this section we will consider some spectral components of the Fourier transformed solution, i.e., for particular k and σ, in response to particular forms of the wind stress forcing. It is based on a similar analysis for atmospheric heating in Salby and Garcia (1987). The spectral components considered will be those relevant in the deep ocean when the forcing frequency is not too high, i.e., Kelvin, Rossby and mixed Rossby–gravity waves. The gravity wave component will not be considered because it is small when σ is not too large; the vertically trapped components with negative equivalent depths also will not be considered because they do not contribute to the propagating solution in the deep ocean. We will consider the energy of these wave modes in transformed space as a function of k, σ, z and magnitude of damping.

In the same spirit as using a constant N profile, i.e., analytic tractability, the damping is chosen to be linear.

The Rayleigh friction coefficient is ν and the Newtonian cooling coefficient κ. Again for convenience ν will be taken equal to κ because in the VP representation this is not a special case; each wave component has meridional phase changes; in contrast to the VS representation. This point and other linear damping wave effects are discussed in section 4. It is now convenient to define a complex frequency ω by

$$\omega = \sigma + i\nu, \quad (29)$$

because the results of section 2 carry over to the damped case with σ replaced by ω. The stress in the forcing layer is chosen to be Gaussian in x, y and t:

$$\tau_z{}^x \text{ or } \tau_z{}^y = \tau^0 \exp\left\{-\left[\frac{\lambda x^2}{2}+\frac{\mu y^2}{2}+\frac{\gamma t^2}{2}\right]\right\}\frac{e(z)}{d}, \quad (30)$$

where $e(z)$ is given in (22) and $x = 0$ is considered as the center of the ocean basin. We now take the Fourier transforms with respect to time and longitude

$$\bar{\tau}_z{}^x(\sigma,k,y,z) = \frac{1}{2\pi}\int_{-\infty}^{\infty}\int_{-\infty}^{\infty}\tau_z{}^x \exp[i(\sigma t - kx)]dxdt. \quad (31)$$

This gives the forcing of the space–time transformed equations as

$$\bar{\tau}_z{}^x \text{ or } \bar{\tau}_z{}^y = \frac{\tau^0}{\sqrt{\lambda\gamma}} \exp\left\{-\left[\frac{k^2}{2\lambda}+\frac{\sigma^2}{2\gamma}+\frac{\mu y^2}{2}\right]\right\}\frac{e(z)}{d}. \quad (32)$$

For positive values of σ and k which result in eastward propagation, the only long-wave propagating solution when $\tau_z{}^x$ is symmetric about the equator is the Kelvin wave.

a. Kelvin wave

The Kelvin wave dispersion relation and eigenfunctions can be found from (15) and (13) by setting $n = -1$:

$$\sqrt{gh}^{-1} = \frac{\omega}{k}, \quad \sigma>0 \quad P^{-1} = \frac{\omega}{k}U^{-1} = \left(\frac{\omega}{k}\right)^2\psi_0(y'),$$

$$V^{-1} = 0, \quad (33)$$

where

$$y' = \left(\frac{\beta k}{\omega}\right)^{1/2} y.$$

When the forcing is in the zonal wind stress, the projection onto the Kelvin wave given by (19) is

$$A_{\sigma k}^{-1} = \frac{\tau^0 \pi^{1/4} k^3}{id\sqrt{\lambda\gamma}\omega^4} \exp\left[-\left(\frac{k^2}{2\lambda}+\frac{\sigma^2}{2\gamma}\right)\right]\int_{-\infty}^{\infty}\exp\left[-\left(\frac{\mu}{2}y^2\right.\right.$$

$$\left.\left.+\frac{\beta k}{2\omega}y^2\right)\right]dy\bigg/\int_{-\infty}^{\infty}\exp\left[-\left(\frac{\beta k}{\omega}y^2\right)\right]dy. \quad (34)$$

Both integrals in (34) are along the real y axis but of

exponentials with complex arguments when friction is present and ω is complex. However, the denominator in (34) can be evaluated as

$$\int_{-\infty}^{\infty} e^{-y^2} dy = \left(\frac{\omega}{\beta k}\right)^{1/2} \int_{-\infty}^{\infty} e^{-y'^2} dy', \qquad (35)$$

where the integral on the right-hand side of (35) is now taken along the real y' axis. This requires taking a contour integral in the complex plane along the contour shown in Fig. 1, noting that the integrand has no poles within the contour and showing that the contributions to the integral along the lines 1 and 2 are zero. The latter requires that 2α, the phase of $\omega/\beta k$, be between $\pm\pi/2$ which is satisfied as long as the frequency is nonzero. There is a similar requirement on the integral in the numerator of (34) which is also satisfied. In general, it will always be satisfied if the forcing has no poles and is well behaved at infinity. Thus

$$A_{\sigma k}^{-1} = \frac{\tau^0 \pi^{1/4} k^3}{id\sqrt{\lambda\gamma}\omega^4} \left[\frac{2}{1 + \dfrac{\mu\omega}{\beta k}}\right]^{1/2} \exp\left[-\left(\frac{k^2}{2\lambda} + \frac{\sigma^2}{2\gamma}\right)\right]. \qquad (36)$$

In order to assess energy as a function of depth, we now define the averaged space–time transformed energy $E_{\sigma k}^n$ of a wave mode as

$$E_{\sigma k}^n = \frac{1}{2}\int_{-\infty}^{\infty}\left[\bar{u}\bar{u}^* + \bar{v}\bar{v}^* + \left(\frac{\bar{p}}{\sqrt{gh^n}}\right)\left(\frac{\bar{p}}{\sqrt{gh^n}}\right)^*\right]dy', \qquad (37)$$

where the overbar denotes the transformed variable and * the complex conjugate. For the Kelvin wave this space–time transformed energy below the forcing layer is

$$E_{\sigma k}^{-1} = \left|\left(\frac{\omega}{k}\right)^3 A_{\sigma k}^{-1} \sin\left(\frac{Nkd}{\omega}\right)\exp\left(\frac{iNkz}{\omega}\right)\right|^2, \qquad (38)$$

where the vertical wavenumber $m = Nk/\omega$. Equation (38) illustrates how forcing and friction affect the space–time transformed energy of a VP Kelvin wave. It shows:
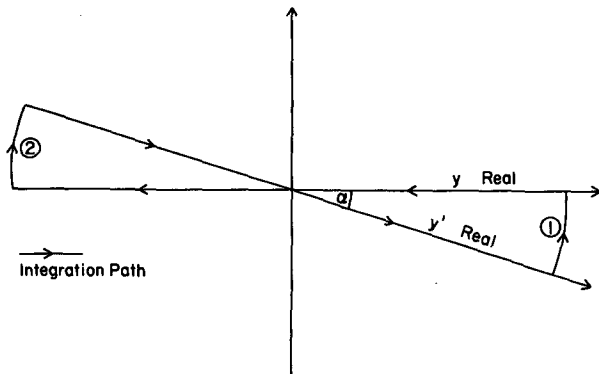
1) The time and longitudinal structure of the forcing affects the energy as the square of the Fourier transform of the forcing. This is independent of the wave being considered. For the Gaussian forcing considered in this section, the Fourier transform (32) is exponentially red when λ and γ are small, large zonal and time scales, and almost white when λ and γ are large, small zonal and time scales.

2) The latitudinal structure affects the energy by the square of the projection (19) onto the particular wave in question. The projection is large when the frequency σ is small and the Kelvin wave is closely trapped around the equator and is small when σ is large and the Kelvin wave is very broad meridionally, i.e., extending well beyond r_z^x.

3) Friction affects the energy through the exponential decay term with depth in (38) which for constant N is

$$\exp[2Nk\nu z/(\sigma^2 + \nu^2)]. \qquad (39)$$

When $\sigma \gg \nu$, the exponential decay coefficient is proportional to the damping coefficient and inversely proportional to σ^2, and the vertical wavenumber varies like σ^{-1}. When σ is small, the Kelvin wave has a smaller vertical wavelength and equivalent depth and decays rapidly with depth. The higher frequency Kelvin waves have large vertical wavelengths and decay slowly with depth. Comments 2 and 3 also hold for the other long VP waves.

An alternative to studying the energy itself is to study the space–time transformed downward energy flux, $\mathrm{Re}(\bar{w}\bar{p}^*)$. Comments 1 and 2 apply exactly to the energy flux because it is also a quadratic quantity. Comment 3 applies exactly when N is constant because the vertical structure function for $\bar{w}$ is the same as for $\bar{u}$, $\bar{v}$ and $\bar{p}$ in this case. Comment 3 and this equivalence do not apply when N is a function of depth.

In order to evaluate the Kelvin wave space–time transformed energy, the dimensional and nondimensional quantities given in Table 1 were chosen. The stress is a Gaussian with equal horizontal e-folding scales of 500 km and an e-folding forcing time scale of either 10 or 30 days. The N and d are kept fixed, but the results depend only upon the product Nd when the depths examined are multiples of d. We use two values of friction, weak and strong, corresponding to spindown times of 1000 and 500 days, two wavenumbers corresponding to wavelengths of 12 500 and 6250 km, and two depths are examined: twice and twenty times the mixed layer depth. The absolute scale on the following figures is arbitrary and depends upon the strength of the wind stress, etc., but the scales are consistent between all the plots showing comparative amplitudes for different waves and the attenuation with depth. Figure 2 shows $E_{\sigma k}^{-1}$ against σ for 10 day e-folding forcing time scale with strong friction at 100 m depth for (a) 12 500 and (b) 6250 km wavelengths. The plot covers a frequency range from zero to 0.4 which is a

FIG. 1. Contour of integration in the complex plane to prove Eq. (35).

TABLE 1. Scales and parameter values.

Dimensional
Length scale l = 250 km, Time scale T = 2 days,
Mixed layer depth = 50 m, β = 2.29 × 10^{-11} m^{-1} s^{-1}
Buoyancy frequency N = 2.8 × 10^{-2} s^{-1}

Nondimensional
λ =　$\mu = \frac{1}{2}$,　$\beta = 1$,　$Nd = -10$

$$\gamma = \begin{cases} \frac{2}{25} & \text{10-day } e\text{-folding forcing time scale} \\ \frac{2}{225} & \text{30-day } e\text{-folding forcing time scale} \end{cases}$$

$$\nu = \begin{cases} \frac{1}{500} & \text{1000 days spindown; weak} \\ \frac{1}{250} & \text{500 days spindown; strong} \end{cases}$$

$$k = \begin{cases} \frac{1}{8} & \text{12 500 km wavelength} \\ \frac{1}{4} & \text{6250 km wavelength} \end{cases}$$

$$z = \begin{cases} 2d & \text{100 m depth} \\ 20d & \text{1 km depth} \end{cases}$$

period of about 30 days and it shows that the energy has several peaks so that several frequencies are important to the solution at this depth. The larger value of k for the shorter wave means that the energy oscillates more rapidly with σ so that Fig. 2b has more peaks than Fig. 2a. Also the amplitude of the shorter wave response is reduced somewhat compared to that of the longer wave, so that the spectrum is red in k. The same plots for 30 day e-folding forcing time scale are shown in Fig. 3. The response is shifted to lower frequencies; σ = 0.2 corresponds to a period of just over 60 days, although the peak response is only shifted slightly to a period of about 120 days. The maximum amplitude of the response is larger than that for the 10 day forcing time scale, and, as in Fig. 2, several frequencies contribute significantly to the response. Figure 3b again

shows the redness of the response in k in that the shorter wave response is reduced compared to the longer wave, and shows that more frequencies contribute significantly to the shorter wave response. These properties are consistent for the shorter Kelvin and Rossby waves, so that only results for the longer waves are shown subsequently. Figure 4 shows plots of $E_{\sigma k}^{-1}$ at 1 km depth for (a) 10 day and (b) 30 day e-folding forcing time scales. It shows that the amplitudes are considerably reduced from those at 100 m, with the response to the 30 day forcing time scale decreasing faster with depth than the response to the 10 day forcing time scale. The maximum response is now shifted to higher frequencies and therefore longer vertical wavelengths than at 100 m and is at different frequencies for the two forcing time scales. Also compared with 100 m only one or two frequencies contribute significantly to the solution, so that observations at this depth may be able to resolve the frequency bands shown in Fig. 4 quite well, which was not the case at 100 m depth. Figure 5 shows the same plots as Fig. 4 but with weak friction. It shows considerably larger amplitudes compared with strong friction results; the maximum responses are at lower frequencies and more frequencies contribute significantly to the solutions.

b. First Rossby wave

The dispersion relation of the first Rossby wave can be found from (15) with $n = 1$:

$$\sqrt{gh^1}$$

$$= \left\{ -3\beta - \left[9\beta^2 + 4\omega^2 \left(k^2 + \frac{\beta k}{\omega} \right) \right]^{1/2} \right\} \bigg/ 2 \left(k^2 + \frac{\beta k}{\omega} \right),$$

$$-\beta/k < \sigma < 0. \quad (40)$$

The eigenfunctions are given by (13) with $n = 1$, and the projection coefficient $A_{\sigma k}^1$ from (19) is given by
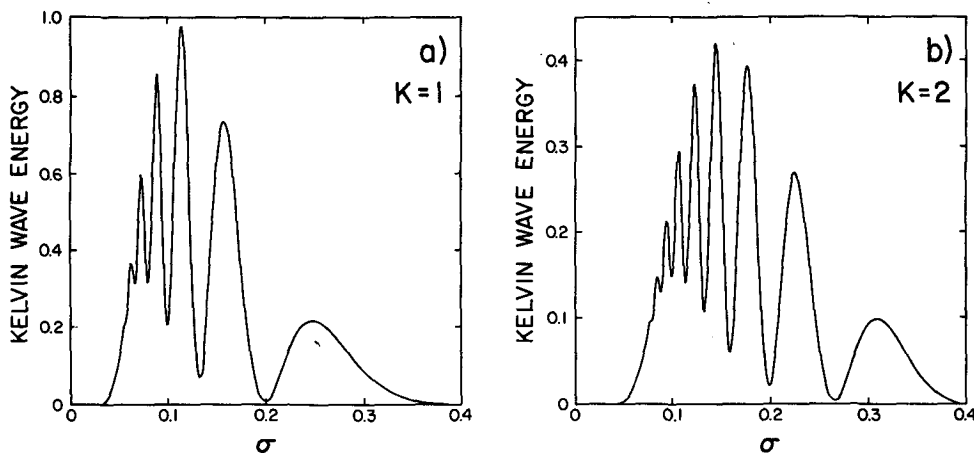

FIG. 2. Space–time transformed Kelvin wave energy vs. frequency at $z = 2d$ for 10-day e-folding forcing time scale, strong friction for (a) 12 500 km wavelength and (b) 6250 km wavelength.
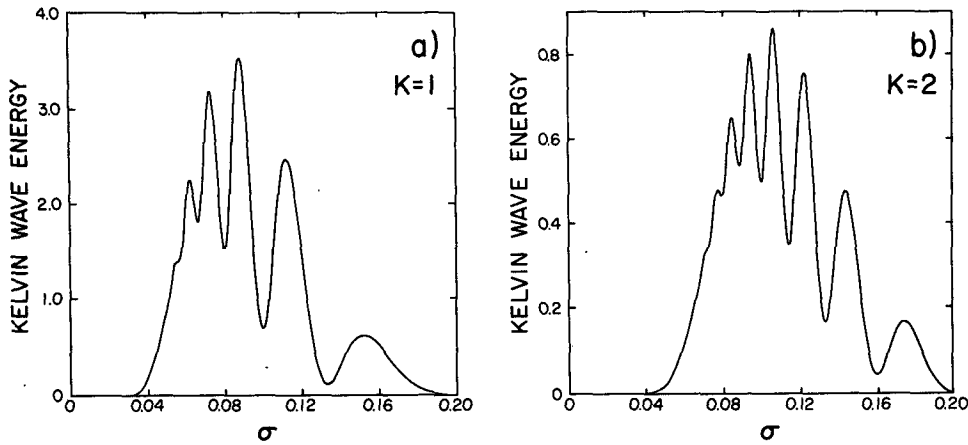
FIG. 3. As in Fig. 2 except for an e-folding forcing time scale of 30 days.

$$A_{\sigma k}^1 = \frac{\tau^0 \pi^{1/4}}{d\sqrt{\lambda\gamma}}$$

$$\times \left[a_1 \left(\frac{2}{1 + \mu\sqrt{gh^1}/\beta} - 1 \right) + b_1 \right] \exp\left[-\left(\frac{k^2}{2\lambda} + \frac{\sigma^2}{2\gamma} \right) \right]$$

$$\times \left\{ i\omega g h^1 \left(1 + \frac{\mu\sqrt{gh^1}}{\beta} \right)^{1/2} (2a_1^2 + b_1^2) \right\}^{-1}. \quad (41)$$

Thus the space–time transformed energy of the first Rossby wave is given by

$$E_{\sigma k}^1 = 2[2a_1 a_1^* + b_1 b_1^* + \omega\omega^*(gh^1)^{1/4}(gh^{1*})^{1/4}/\beta]$$

$$\times \left| gh^1 A_{\sigma k}^1 \sin\left(\frac{Nd}{\sqrt{gh^1}} \right) \exp\left(\frac{iNz}{\sqrt{gh^1}} \right) \right|^2. \quad (42)$$

Figure 6 shows plots of $E_{\sigma k}^1$ against σ for the 12 500 km wavelength with strong friction at a depth of 100 m for (a) 10 day e-folding and (b) 30 day e-folding forcing time scales. The amplitude of the first Rossby

wave response is larger than that of the Kelvin wave and its maximum amplitude is also larger for the 30 day than the 10-day forcing time scale. The maximum response is at a lower frequency for the 30-day than the 10-day forcing time scale and both are at lower frequencies than the maximum Kelvin wave response. Several frequencies contribute significantly to the solution at this depth. Figure 7 shows the corresponding plots at a depth of 1 km. Comparison with Fig. 4 shows that the first Rossby wave is attenuated with depth less quickly than the Kelvin wave because of its larger equivalent depth or smaller vertical wavenumber for given values of σ and k. As for the Kelvin wave, the dominant response compared to 100 m is shifted to higher frequencies and therefore longer vertical wavelengths, and is simplified in that only one or two frequencies contribute significantly to the solution. Again the response to the 30-day forcing time scale decays more quickly with depth than the response to the 10-day forcing time scale.

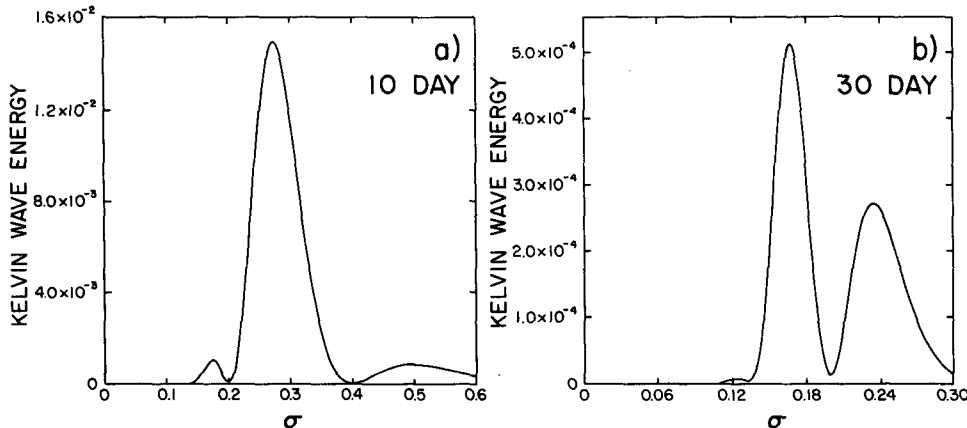Higher mode Rossby waves will have larger equiv-

FIG. 4. Space–time transformed Kelvin wave energy vs. frequency at $z = 20d$ for 12 500 km wavelength, strong friction for (a) 10-day e-folding and (b) 30-day e-folding forcing time scales.
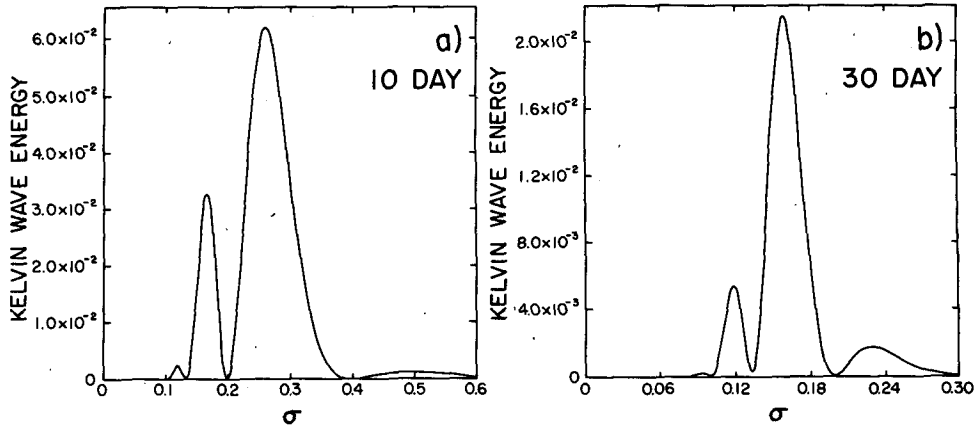
FIG. 5. As in Fig. 4 except for weak friction.

alent depths or smaller vertical wavenumbers than the first Rossby wave. Their responses will oscillate less rapidly with σ so that, at any given depth, fewer frequencies contribute significantly to the solution, and their responses will decay less rapidly with depth than for the first Rossby wave. However, the latitudinal scale of these higher mode Rossby waves increases quickly and the projection coefficient (19) decreases compared to (41) for the first Rossby wave.

c. Mixed Rossby–gravity wave

This wave has the opposite latitudinal symmetry than the other waves considered, so that now the forcing is assumed to have zero $\tau_z{}^x$ and nonzero $\tau_z{}^y$. The dispersion relation of the mixed Rossby–gravity wave is found from (15) with $n = 0$:

$$\sqrt{gh^0} = \omega^2/(\beta + \omega k), \quad \sigma > -\beta/k, \tag{43}$$

and the corresponding eigenfunctions are given by (13) with $n = 0$ ignoring the second terms in P^0 and U^0.

The projection coefficient from (19) is given by

$$A^0_{\sigma k} = \left(\frac{2}{\lambda\gamma}\right)^{1/2} \frac{\tau^0\pi^{1/4}}{d\omega^4}\left(\frac{\beta^2}{gh^0}\right)^{3/4}\left(1 + \frac{\mu\sqrt{gh^0}}{\beta}\right)^{-1/2}$$

$$\times \exp\left[-\left(\frac{k^2}{2\lambda} + \frac{\sigma^2}{2\gamma}\right)\right], \tag{44}$$

and the mixed Rossby–gravity wave energy by

$$E^0_{\sigma k} = \frac{2\omega\omega^*}{\beta^2}[\omega\omega^* + \beta(gh^0)^{1/4}(gh^{0*})^{1/4}]$$

$$\times \left|gh^0 A^0_{\sigma k}\sin\left(\frac{Nd}{\sqrt{gh^0}}\right)\exp\left(\frac{iNz}{\sqrt{gh^0}}\right)\right|^2. \tag{45}$$

In the low-frequency limit, the equivalent depth of the mixed Rossby–gravity wave is much smaller than that of the Kelvin wave so that (i) it is tightly trapped about the equator, (ii) the response at 100 m (not shown) oscillates very rapidly with σ so that very many frequencies contribute significantly to the solution, and
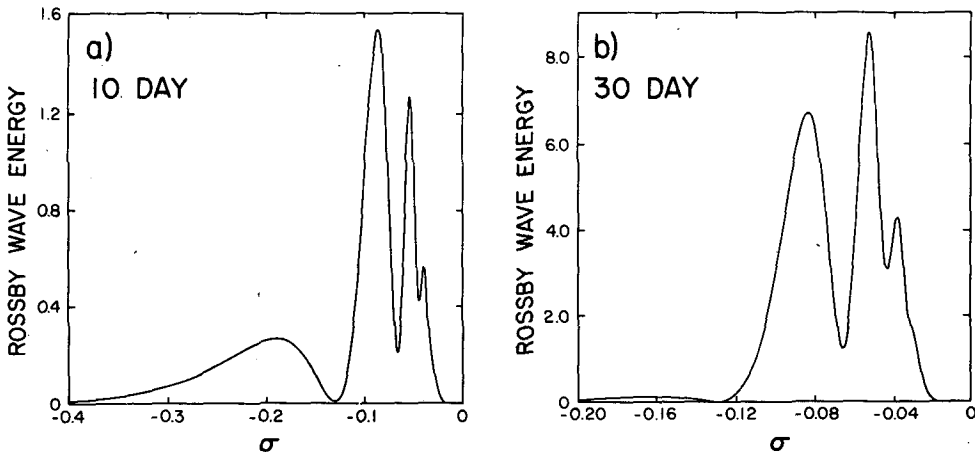

FIG. 6. Space–time transformed first Rossby wave energy vs frequency at $z = 2d$ for 12 500 km wavelength, strong friction for (a) 10-day e-folding and (b) 30-day e-folding forcing time scales.
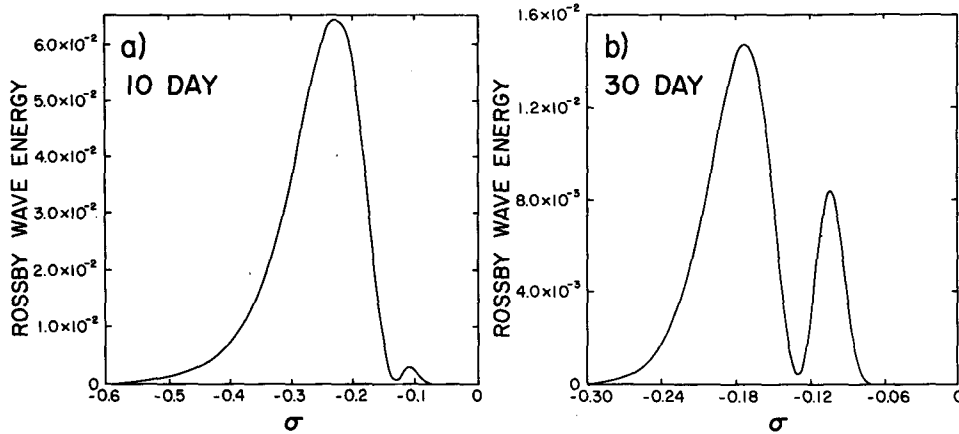
FIG. 7. As in Fig. 6 except at a depth of $z = 20d$.

(iii) the response decays very rapidly with depth. The last point is illustrated in Fig. 8 which shows plots of $E_{\sigma k}^0$ against σ for the 12 500 km wavelength with weak friction at a depth of 1 km for (a) 10-day e-folding and (b) 30-day e-folding forcing time scales. Figure 8 shows the very small amplitudes especially for the 30 day forcing time scale and that several frequencies contribute significantly to the solution even at 1 km. The dominant responses are at higher frequencies than for the Kelvin and first Rossby waves. In contrast to the Kelvin and Rossby waves, the maximum amplitude of the mixed Rossby–gravity wave response is much larger for the 10-day than the 30-day forcing time scale, and the shorter wave response is increased compared to the longer wave response.

d. Gravity waves

The equivalent depth of the first gravity wave is given by (40) but with a plus sign before the square root term rather than a minus sign, and is smaller than that of the Rossby–gravity wave. Thus (i) it is very tightly trapped about the equator, (ii) the response oscillates more rapidly with σ and (iii) the response decays even more rapidly with depth than the mixed Rossby–gravity wave response. These tendencies become even more acute for higher mode gravity waves, so that no plots of space–time transformed gravity wave energy are shown.

4. Linear damping effects on VP and VS waves

The solutions in the last section were calculated using linear damping with the Prandtl number ($\text{Pr} = \nu/\kappa$) set equal to one. The effects of linear damping on VP waves are explored further in this section and compared and contrasted with the effects on VS waves.

For a VP wave, σ and k are real and the addition of Rayleigh friction modifies the dispersion relation (15) by replacing σ by $\sigma + i\nu$. This relation is solved for the eigenvalue $\sqrt{gh''}(\sigma, k, \nu)$, which now becomes complex. This affects the eigenfunctions (13) because y' from
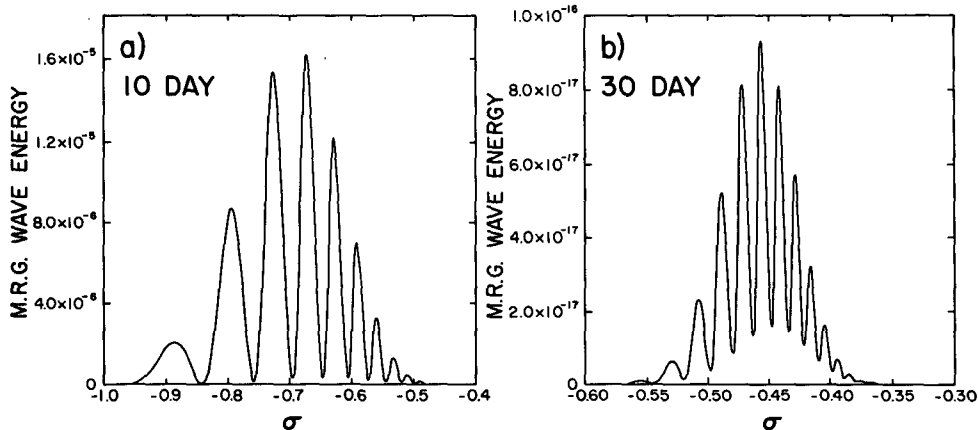

FIG. 8. Space–time transformed mixed Rossby–gravity wave energy vs frequency at $z = 20d$ for 12 500 km wavelength, weak friction for (a) 10-day e-folding and (b) 30-day e-folding forcing time scales.

(14) is now complex so that there are meridional phase changes in the Hermite functions (14) which oscillate very rapidly as $y \rightarrow \pm\infty$. The eigenfunctions which have $\mathrm{Re}(\sqrt{gh^n}) < 0$ will also be complex. Addition of Newtonian cooling affects the vertical structure equation (21) so that the vertical wavenumber $m(\sigma, k, \nu, \kappa)$ from (23) also becomes complex. This means that the vertically propagating waves decay in the vertical as analyzed in section 3, see (39), and that the solutions (24) trapped near the surface oscillate slowly in the vertical. This analysis shows that, in general when linear damping is present, there are meridional phase changes in each wave component of the VP representation. The special case in the VP representation, when there are no meridional phase changes in each wave component, occurs when $\nu = 0$ whatever the value of κ. This fact was exploited by Salby and Garcia (1987) who incorporated only thermal damping and so used the inviscid set of horizontal eigenfunctions. As mentioned in section 3, the $\mathrm{Pr} = 1$ case is not special in the VP representation because each wave component has meridional phase changes for this value of Pr.

In the VS representation the effect on a single wave component is different; σ and gh^n are now real and the dispersion relation is solved for the eigenvalue $k(\sigma, gh^n, \nu, \kappa)$, which becomes complex. The decay in each component is in the zonal direction rather than in the vertical. Yamagata and Philander (1985) analyze the general case and show that each wave again has phase changes in y. However, the phase changes are different than in the VP representation because they depend upon both ν and κ rather than just ν, as in the VP representation. In the VS representation, meridional phase changes in each wave component do not occur either when $\mathrm{Pr} = 1$, which is the special case in the VS representation, or when $\sigma = 0$ and the solution is steady.

This difference in the meridional phase changes in each wave component due to linear damping in the VP and VS representations seems to have been overlooked in previous studies of the linear damping effects on equatorial waves, several of which are listed in Table

2. The VP wave entries in Table 2 are Chang (1977) who studied the Kelvin wave when $\mathrm{Pr} = 1$, Stevens and White (1979) who extended this to arbitrary values of Pr and Chang and Lim (1982) who gave the general solution for Rossby and gravity waves. The mixed Rossby–gravity wave dispersion relation is (43). The VS entries in Table 2 are Martinsen and Weber (1981) who studied the Kelvin wave in the presence of Rayleigh friction only, Mofjeld (1981) who studied all waves in the same situation, and Yamagata and Philander (1985) who studied all waves in the general case of arbitrary Pr. Meridional phase changes in a single wave component based on linear damping effects are discussed in all the papers listed in Table 2 except for Stevens and White (1979).

In general, in forced wave problems it is fallacious to make conclusions about the total forced solution based upon the response in each wave component. For example, linear damping affects each VS and VP wave component quite differently, yet the total solution summed over all the wave components in the two representations is the same. This fallacy is especially true about phase changes in y; consider a solution when $\mathrm{Pr} = 0$ or 1 when one representation has phase changes in y for each wave component and the other representation does not. The true phase changes in y only become clear when all the wave components in the representations have been summed.

5. Discussion and conclusions

This paper attempts to answer the question of how forcing, linear friction and the body force assumption affect the vertical propagation of energy in the equatorial oceans. Section 2 shows that the time and longitudinal structure of the forcing affects all VP waves in the same way through the Fourier transforms in t and x, respectively. The meridional structure of the forcing affects each individual VP wave differently through the projection in y onto that wave component. A new expression for this projection onto the pressure

TABLE 2. Waves with linear damping.

Reference	Wave type	Raleigh friction	Newtonian cooling	Prandtl number	Complex σ?	Complex k?	Complex y-scale?	Complex m?
Chang (1977)	VP Kelvin	Yes	Yes	1	No	No	Yes	Yes
Stevens and White (1979)	VP Kelvin	Yes	Yes	Any	No	No	Yes[†]	Yes
Chang and Lim (1982)	VP Rossby and gravity	Yes	Yes	Any	No	No	Yes[†]	Yes
Martinsen and Weber (1981)	VS Kelvin	Yes	No	∞	Yes	No	Yes	No
Mofjeld (1981)	VS all	Yes	No	∞	No	Yes	Yes	No
Yamagata and Philander (1985)	VS all	Yes	Yes	Any	No	Yes	Yes[*]	No

[†] In general yes, but no when the Prandtl number is zero.
[*] In general yes, but no either when the Prandtl number is one or for steady forcing with any Prandtl number.

equation, when the forcing is in the momentum equations, is given by the right-hand side of (19). In section 3, the transforms and projections for the Kelvin, first Rossby and mixed Rossby–gravity waves are derived explicitly for forcings that are Gaussian in t, x and y. The effects of other forcings can be written explicitly if the Fourier transforms in t and x and the projection in y onto the Hermite functions can be done analytically.

The effects of linear friction and the body force assumption studied in sections 2 and 3 can be determined analytically when the buoyancy frequency is assumed to be constant. When N is constant and the damping is small compared to the frequency, friction decreases the response amplitude exponentially with depth, with a coefficient proportional to the damping magnitude. As the response propagates to greater depths, friction moves the maximum response to higher frequencies and simplifies it because fewer frequencies contribute significantly to the response. In section 2 the solution well below the forcing is derived for four different profiles of stress forcing in the mixed layer. The behavior in the long vertical wavelength limit as $m \rightarrow 0$ is the same for all four profiles and the behavior as $m \rightarrow \infty$ decays less rapidly when the body force is uniform than for the other three profiles. However, the forcing projects strongly onto the modes with small m and only weakly onto those with large m. This suggests that the rate of vertical propagation of energy is insensitive to the precise choice of body force profile.

These conclusions have implications for the analysis of equatorial observations that have been Fourier transformed in time and longitude. They imply that the resulting spectrum with vertical wavenumber m should be red. If the observations are just below the forcing then they will be complicated because many different wave components will be emphasized at several frequencies and zonal wavenumbers. If the observations are deeper in the ocean, however, then the forced response has had time to disperse in space and for friction to act. Thus the observations will be simpler as fewer wave components will dominate at fewer and higher frequencies, which have corresponding longer vertical wavelengths. The situation is analogous to observations taken in the tropical stratosphere. Just above the tropopause several different wave types with vertical wavelengths of 10 km or less have been identified. Higher in the stratosphere Kelvin waves with higher frequencies and longer vertical wavelengths have been identified; see Salby and Garcia (1987). Of course dispersion of the response to localized forcing also occurs in space and time. To the east of the forcing only Kelvin, mixed Rossby–gravity and gravity wave components will be seen, and Rossby waves will only be seen to the west of the forcing. If the observations are taken almost directly below the forcing then only the high frequency response will be seen, whereas if the observations are taken at almost the same depth as the forc-

ing then only the low frequency response will be seen. Also the latitudinal position of the observations is important as only wave components with a significant amplitude at that latitude will be seen. Finally when the response is seen in time depends upon the distance from the forcing and the group velocity of the wave component being observed.

These conclusions are based upon a constant N assumption and are only valid well away from the forcing in an ocean of infinite extent with no mean flow. This is unrealistic in the equatorial oceans where the buoyancy profile has a large maximum in the shallow thermocline. Gent and Luyten (1985) studied the effect of realistic N profiles and concluded that they can have a very strong reflection effect on the vertical propagation of energy, whereas the study of Rothstein et al. (1985) suggests a much smaller effect. Gent and Luyten (1985) conclude that models with constant N give unrealistic results for vertical energy propagation, but, even so, this assumption is used in this paper in order to get analytic forms for the effects of friction and the body force assumption. Wave reflections from ocean boundaries will also be important if the forcing time scale is much longer than the values considered in this paper. McPhaden et al. (1986) show that realistic mean flows can also drastically affect the character of vertical energy propagation in the equatorial oceans. Ideally all effects should be included in a more comprehensive model.

Section 4 shows that linear damping effects are very different on each VP or VS wave component. A VP wave decays with depth but not in longitude whereas a VS wave decays in longitude but not with depth. In general, both waves have phase changes in latitude but they are different in the two wave types. However, the two representations give the same solution to a general forced problem, so that it is fallacious to make deductions about meridional phase changes in the total solution from the phase changes of each wave component.

REFERENCES

Abramowitz, M., and I. A. Stegun, 1964: *Handbook of Mathematical Functions.* Dover.
Chang, C. P., 1977: Viscous internal gravity waves and low-frequency oscillations in the tropics. *J. Atmos. Sci.,* **34,** 901–910.
——, and H. Lim, 1982: On the effects of viscous damping on equatorial Rossby waves. *J. Atmos. Sci.,* **39,** 1726–1733.
Gent, P. R., and J. R. Luyten, 1985: How much energy propagates

vertically in the equatorial oceans? *J. Phys. Oceanogr.,* **15,** 997–1007.

Knox, R. A., and D. Halpern, 1982: Long range Kelvin wave propagation of transport variations in Pacific ocean equatorial currents. *J. Mar. Res.* **40**(Suppl), 329–339.

Lukas, R., S. P. Hayes and K. Wyrtki, 1984: Equatorial sea level response during the 1982–83 El Niño. *J. Geophys. Res.,* **89,** 10 425–10 430.

Martinsen, E. A., and J. E. Weber, 1981: Frictional influence on internal Kelvin waves. *Tellus,* **33,** 402–410.

McPhaden, M. J., J. A. Proehl and L. M. Rothstein, 1986: The interaction of equatorial Kelvin waves with realistically sheared zonal currents. *J. Phys. Oceanogr.,* **16,** 1499–1515.

Mofjeld, H. O., 1981: An analytic theory on how friction affects free internal waves in the equatorial waveguide. *J. Phys. Oceanogr.,* **11,** 1585–1590.

Philander, S. G. H., 1978: Forced oceanic waves. *Rev. Geophys. Space Phys.,* **16,** 15–46.

Rothstein, L. M., D. W. Moore and J. P. McCreary, 1985: Interior reflections of a periodically forced equatorial Kelvin wave. *J. Phys. Oceanogr.,* **15,** 985–996.

Salby, M. L., and R. Garcia, 1987: Transient response to localized episodic heating in the tropics. Part I: Excitation and short-time near-field behavior. *J. Atmos. Sci.,* **44,** 458–498.

Stevens, D. E., and G. H. White, 1979: Comments on "Viscous internal gravity waves and low-frequency oscillations in the tropics". *J. Atmos. Sci.,* **36,** 545–546.

Wunsch, C., 1977: Response of an equatorial ocean to a periodic monsoon. *J. Phys. Oceanogr.,* **7,** 497–511.

Yamagata, T., and S. G. H. Philander, 1985: The role of damped equatorial waves in the oceanic response to winds. *J. Oceanogr. Soc. Japan,* **41,** 345–357.